Chemical Physics 400 (2012) 126–136

Contents lists available at SciVerse ScienceDirect

Chemical Physics

journal homepage: www.elsevier.com/locate/chemphys

Anharmonic Franck–Condon simulation of the absorption and fluorescence spectra for the low-lying S_1 and S_2 excited states of pyrimidine

Ling Yang [a,b,c], Chaoyuan Zhu [a,*], Jianguo Yu [c,*], Sheng Hsien Lin [a]

[a] Department of Applied Chemistry, Institute of Molecular Science and Center for Interdisciplinary Molecular Science, National Chiao-Tung University, Hsinchu 30050, Taiwan
[b] Institute of Theoretical and Simulation Chemistry, Academy of Fundamental and Interdisciplinary Science, Harbin Institute of Technology, Harbin 150080, PR China
[c] Department of Chemistry, Beijing Normal University, Beijing 100875, PR China

ARTICLE INFO

Article history:
Received 9 August 2011
In final form 14 March 2012
Available online 3 April 2012

Keywords:
Harmonic and anharmonic simulation
Franck–Condon factors
Reorganization energy
Absorption and fluorescence spectra
Vibronic spectra

ABSTRACT

Intensities and profiles of vibronic spectra of the low-lying singlet excited states were investigated with anharmonic and harmonic Franck–Condon simulations for pyrimidine. The first-order anharmonic correction shows dynamic shift of spectra that is exactly same as difference of reorganization energy between ground and excited states. The first-order correction show intensity enhancement of absorption and intensity weakening of fluorescence for S_1 state, and dynamic shift is also significant. On the other hand, the first-order correction is negligible for S_2 state. The main spectral progressions are well described by totally symmetry modes ν_{6a}, ν_1 and ν_{12}. One mode from non-total symmetry ν_{16a} contributes to the weak band at $16a^2$ transition for S_1 state. Four ab initio methods were employed in simulation; CASSCF, CASPT2, DFT and TD-DFT, and coupled-cluster singles-doubles (CCSD) and the equation-of-motion (EOM-CCSD) methods. They all work well, but CASSCF method show the best agreement with experiment for the weak-band intensities.

1. Introduction

Ab initio quantum chemistry methods provide a powerful tool to simulate molecular spectroscopy and dynamics. Two major steps are generally made for simulation. The first part is statics in which molecular structures, vibrational frequencies and transition energies are calculated within Born–Oppenheimer approximation for electronically ground and excited states. The second part is dynamics in which wavefucntion overlap between ground and excited states is computed within Franck–Condon (FC) approximation [1–3]. These theoretical simulations can be very helpful for interpreting experimental observations such as electronic spectra like VUV absorption, fluorescence, and the other nonradiative processes like electron and energy transfer. Exact simulation for multidimensional FC overlap integrals is not practical for many-atom systems. Harmonic approximation with normal mode analysis is commonly utilized for simulation and anharmonic correction may be included for improvement. Further approximations are usually introduced for practical simulation like displaced oscillator approximation, distorted oscillator approximation, and normal mode-mixing with including Duschinsky effect [4]. Various analytical and numerical methods have been developed to compute FC overlap integrals with various applications [5–35].

Pyrimidine (1,3-diazine), $C_4H_4N_2$, belongs to the group of diazine ring molecules, whose skeletons serve as building blocks in nature, that may be used as a chemical or molecular model for the single nucleosides (thymine, cytosine and uracil) in nucleic acids [36–39]. The electronic spectroscopy of the azabenzenes (pyridine, pyrazine and pyrimidine) has been very interesting subject due to its rich excited-state dynamical and photochemical properties [36,40,41], as well as its importance for biologically relevant spectroscopic processes [42,43]. A variety of computational simulations have been carried out for the S_1 and S_2 absorption and the fluorescence spectra of pyridine [41,44,45] and pyrazine [46,47].

Pyrimidine molecule has been studied by both experimental measurements and theoretical simulations for its low-lying excited states with applications of photophysics and photochemistry. VUV photoabsorption spectrum has been experimentally studied [36,38,39] and ab initio calculation within the level of multi-reference configuration interaction method has been reported as well [48]. More recently, high resolution VUV photoabsorption spectrum has been obtained by Ferreira da Silva [49]. These studies suggested that the low-lying excited states (S_1 and S_2) have C_{2v} group symmetry with transition types of $^1B_1$ ($n \rightarrow \pi^*$) and $^1B_2$ ($\pi \rightarrow \pi^*$), respectively. In addition, Knight et al. [50] carried out extensive analysis of the emission spectrum by exciting a number

* Corresponding authors.
E-mail addresses: cyzhu@mail.nctu.edu.tw (C. Zhu), jianguo_yu@bnu.edu.cn (J. Yu).

0301-0104/$ - see front matter © 2012 Elsevier B.V. All rights reserved.
http://dx.doi.org/10.1016/j.chemphys.2012.03.010

of selectively vibronic levels in the lowest excited ($n \leftarrow \pi^*$) singlet state. Computational studies have been carried out for equilibrium geometries, vibrational frequencies, and ground and low-lying excited state spectra of pyrimidine [51–59]. Malmqvist et al. [57] performed ab initio quantum chemistry studies for number of vertically excited singlet states of pyrimidine. Billes et al. [58] measured and calculated vibrational frequencies at the Møller–Plesset perturbation and density functional theory levels. Later on, symmetry adapted cluster-configuration interaction (SAC-CI) [51] and equation of motion coupled-cluster (EOM-CC) [52–56] methods were adopted to produce fairly high accuracy for excitation energies. Fischer et al. [56] presented not only new experimental data for the lowest excited singlet and triplet states but also high-level calculations ((EOM-CCSD, CASPT2, and CIS) and density functional (B3LYP and TD-B3LYP)) for the first eight singlet and triplet valence excited states of pyrimidine. Åsbrink et al. [60] reported the photoelectron spectra of pyrimidine and other azabenzenes up to 25 eV excitation energy, where the lowest ionization energy was attributed to the removal of an electron from the nitrogen lone pairs. Calculations based on response theory were utilized for calculating two-photon absorption spectra of the lowest electronic states by Luo et al. [59]. A main propose in the present study is to simulate intensities and profiles of vibronic manifold spectra of the low-lying singlet excited states, and to treat absorption and fluorescence in an equal footing by anharmonic Franck–Condon overlapping integrals. The present anharmonic correction can show how intensities and profiles of spectra changes simultaneously for both absorption and fluorescence.

In the present study, we first calculate the equilibrium geometries, vibrational frequencies, vertical and adiabatic excitation energies of the ground state $S_0(^1A_1)$ and the low-lying $S_1(^1B_1)$ and $S_2(^1B_2)$ excited states using CASSCF, CASPT2, CCSD/EOM-CCSD, and DFT/TD-DFT methods. It should be noted that the variational principle in ab initio quantum chemistry methods can insure better accuracy for excitation energies with higher level method but it does not guarantee better accuracy for equilibrium geometries. Intensities and profiles of vibronic spectra in terms of the Franck–Condon overlapping integrals are most sensitive to geometry difference between excited and ground states. Therefore, the CASSCF method can provide accurate vibronic spectra since it treats electronic ground and excited states in an equal footing and it is especially good for geometry optimization of aromatic molecules in which resonance structures are essential. Then, we simulate the absorption and fluorescence spectra for $S_1(^1B_1)$ state and the absorption spectrum for $S_2(^1B_2)$ state by employing the displaced harmonic oscillator approximation including the first-order anharmonic effect. Furthermore, we analyze the distorted effect that takes into account contribution from non-totally symmetry normal modes and it can be considered as diagonal-part correction of Duschinsky mode-mixing matrix. With analytical formulation of absorption and fluorescence coefficients [35], we can explicitly demonstrate how anharmonic effect influences the shifts of spectral peaks, relative intensities and profiles of spectra with respect to harmonic Franck–Condon simulation.

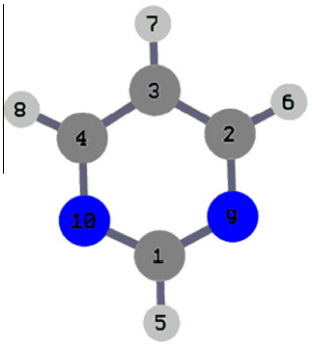

Fig. 1. Atom numbering for pyrimidine.

In Section 2, we briefly introduce ab initio methods for calculation of electronic structures and normal-mode frequencies of the ground and two low-lying singlet excited states of pyrimidine. The displaced harmonic approximation with including the first-order anharmonic correction is also discussed for Franck–Condon factors. In Section 3, the simulated results of electronic structures, absorption and fluorescence spectra are reported along with comparison to experimental observations as well as the some other theoretical simulations. Concluding remarks are given in Section 4.

2. Ab initio methods and anharmonic Franck–Condon factor

2.1. Ab initio methods

Gaussian03 [61] and Molcas 7.5 [62] program packages were employed for calculating the electronic structures of the ground state ($S_0(^1A_1)$) and the first two low-lying singlet excited states ($S_1(^1B_1)$ and $S_2(^1B_2)$). Numbering of atoms is given in Fig. 1. The equilibrium geometries for these three electronic states were calculated at CASSCF(6,6) level with consideration that pyrimidine consists of 6 active electrons and 6 active orbitals including 3 doubly occupied orbitals and 3 virtual orbitals. We have done the other combinations of active electrons and orbitals to test structure calculations and the results verify consistency of the present choice. As the dynamic correlation effects are not included in CASSCF method, we have done CASPT2 and MP2 corrections for both excitation energies and vibrational normal mode frequencies at CASSCF optimized geometries. On the other hand, we have employed the CASPT2, B3LYP/TD-B3LYP, and CCSD/EOM-CCSD methods to calculate the equilibrium geometries of three electronic states, and corresponding vertical excitation energies as well as normal model frequencies. Basis sets of 6-311++g** and aug-cc-pVDZ [63] were adopted in cooperation with the methods mentioned above. The TD-B3LYP and EOM-CCSD methods [64] have been performed using G09 [65] program. All 24 normal-mode frequencies for three electronic states were computed to confirm the optimized geometries as true minima corresponding to their potential energy surfaces. The anharmonic parameters were computed for the ground state with using MP2 and B3LYP methods in both G03 and G09 programs, respectively.

2.2. Anharmonic Franck–Condon factor

We start with perturbation expansion of the jth vibrational normal-mode potential energy as [35]

$$V_j(Q) = a_{j2}Q_j^2 + \lambda a_{j3}Q_j^3 + \lambda^2 a_{j4}Q_j^4 + \cdots \tag{1}$$

in which λ is chosen as a perturbation parameter and Q_j is mass-weighted normal-mode coordinate. The first-order correction in perturbation is zero for energy, but is nonzero for wave function with which absorption coefficient is analytically derived as [35],

$$\alpha(\omega) = \frac{2\pi\omega}{3h}|\vec{\mu}_{ba}|^2 \int_{-\infty}^{\infty} dt e^{it(\omega_{ba}+\Omega_0-\omega)-\gamma_{ba}|t|} \times \exp\left[-\sum_j S_j(1+3\eta_j)\{2\bar{\upsilon}_j + 1 - (\bar{\upsilon}_j+1)e^{it\omega_j} - \bar{\upsilon}_j e^{-it\omega_j}\}\right] \tag{2}$$

for excitation from electronic ground state a to excited state b that means $\omega_{ba} > 0$ in Eq. (2) for adiabatic energy gap between b and a. Fluorescence coefficient is analytically derived as well [35]

$$I(\omega) = \frac{2\pi\omega}{3\hbar}|\vec{\mu}_{ba}|^2 \int_{-\infty}^{\infty} dt e^{-it(|\omega_{ba}|+\Omega_0-\omega)-\gamma_{ba}|t|} \times \exp\left[-\sum_j S_j(1-3\eta_j)\{2\bar{\upsilon}_j+1-(\bar{\upsilon}_j+1)e^{it\omega_j}-\bar{\upsilon}_j e^{-it\omega_j}\}\right] \quad (3)$$

for excitation from electronic excited state a to ground state b that means $\omega_{ba} < 0$ in Eq. (3) for adiabatic energy gap between b and a. Other quantities are same for both Eqs. (2) and (3), where $\bar{\nu}_j = (e^{\hbar\omega_j/k_BT}-1)^{-1}$ is the average phonon distribution, γ_{ba} represents the dephasing constant (with relation to the lifetime $\tau_{ba} = 1/\gamma_{ba}$) between two electronic states, and $\vec{\mu}_{ba}$ is the electronic transition dipole moment. The most important quantities Ω_0 and η_j stand for the first-order anharmonic correction given by

$$\Omega_0 = -2\sum_j \eta_j S_j \omega_j \quad (4)$$

and

$$\eta_j = \frac{a_{j3}d_j}{a_{j2}} = \frac{a_{j3}d_j}{0.5\omega_j^2} \quad (5)$$

where ω_j is harmonic vabrational normal-mode frequency, and the Huang–Rhys factor S_j, the displacement d_j, the second coefficient a_{j2} and the third coefficient a_{j3} of potential energy in Eq. (1) are defined as

$$S_j = \frac{1}{2\hbar}\omega_j d_j^2 \quad (6)$$

$$d_j = Q_j' - Q_j = \sum_n L_{jn}(q_n' - q_n) \quad (7)$$

$$a_{j2} = \frac{1}{2}\frac{\partial^2 V}{\partial Q_j} = \frac{1}{2}\omega_j^2 \quad (8)$$

and

$$a_{j3} = \frac{1}{3!}\frac{\partial^3 V}{\partial Q_j^3} = \frac{1}{3}K_{j3} \quad (9)$$

Inserting Eq. (9) into Eq. (5) leads to

$$\eta_j = \frac{2K_{j3}d_j}{3\omega_j^2} = \frac{K_{j3}d_j^3}{3S_j\hbar\omega_j} \quad (10)$$

The q_n' and q_n in Eq. (7) are the mass-weighted Cartesian coordinates at the equilibrium geometries of the electronic excited and ground states, respectively. Transformation matrix **L** in Eq. (7) can be computed with frequency calculation in G03 and G09 programs. If the dimensionless first-order anharmonic parameter η_j is equal to zero, the absorption and fluorescence coefficients in Eqs. (2) and (3) are exactly same as those in displaced harmonic oscillator approximation. An anharmonic parameter η_j in Eq. (10) is expressed in terms of the diagonal element K_{j3} of cubic force constant estimated from G03 and G09 programs. The displacement d_j in Eq. (7) that is sensitive to geometry differences between two electronic states is essentially parameter to determine intensities and profile of vibronic spectra.

The effective Huang–Rhys factors in Franck–Condon factors are no longer the same from the first-order anharmonic correction; $S_j' = (1 \pm 3\eta_j)S_j$ (+ for absorption in Eq. (2) and – for fluorescence emission in Eq. (3)). Immediate consequence is that mirror image between absorption and fluorescence spectra is broken down accompanying with intensity enhancement of absorption against weakening of fluorescence (or vice versa). At the same time, the harmonic 0–0 excitation energy is shifted by Ω_0 and this can be interpreted as a dynamic correction to spectral position. However, the first-order correction influences little change of band shape in vibronic spectra and for detailed band-shape change the second-order correction is necessary along with the effect like Duschinsky mode-mixing.

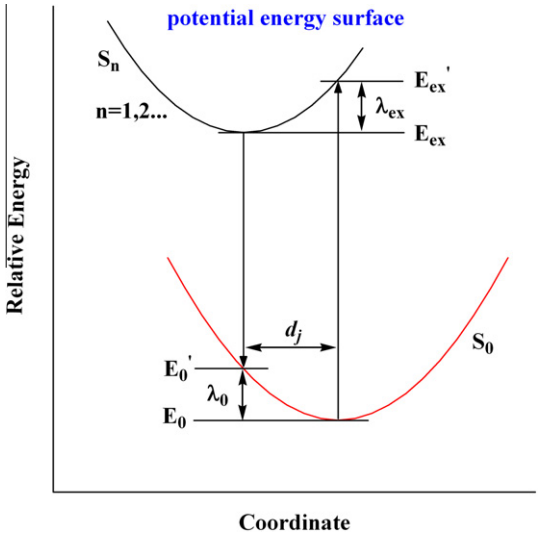

Fig. 2. The ground and excited states reorganization energy from the potential energy surfaces, $\lambda_0 = E_0' - E_0$ and $\lambda_{ex} = E_{ex}' - E_{ex}$.

The first-order anharmonic correction can affect the reorganization energy of ground state ($\lambda_0 = E_0' - E_0$) and excited state($\lambda_{ex} = E_{ex}' - E_{ex}$) as shown in Fig. 2. In comparison with ground-state potential energy defined in Eq. (1), excited-state potential energy is defined as the left-handed shift with respect to ground state

$$V_{ex-j}(Q_j') = a_{j2}(Q_j + d_j)^2 + \lambda a_{j3}(Q_j + d_j)^3 + \lambda^2 a_{j4}(Q_j + d_j)^4 + \cdots \quad (11)$$

for derivation of absorption and fluorescence coefficient in Eqs. (2) and (3). By adding each-mode contribution to reorganization energy together, we derive expression of reorganization energy within the first-order anharmonic correction as

$$\lambda_0 = \sum_j S_j\hbar\omega_j(1-\eta_j) \quad (12)$$

and

$$\lambda_{ex} = \sum_j S_j\hbar\omega_j(1+\eta_j) \quad (13)$$

from which we can immediately find that the reorganization energy differences between the excited state and the ground state is exactly equal to the dynamic shift $\Omega_0 = \lambda_0 - \lambda_{ex}$ in Eq. (4), and this is zero within harmonic case.

3. Results and discussion

3.1. Equilibrium geometries of S_0, S_1, and S_2 states

We optimized the equilibrium geometries of three electronic states (the ground state ($S_0(^1A_1)$) and the first two low-lying singlet excited states ($S_1(^1B_1)$ and $S_2(^1B_2)$) using CAS(6,6)/6-311++g**, CASPT2/aug-cc-pVDZ, CCSD/EOM-CCSD/cc-pVDZ and B3LYP/TD-B3LYP/6-311++g** methods. The measurements from gas-phase electron diffraction, rotational spectroscopy, and liquid–crystal NMR [66] predicted that the ground state of pyrimidine molecule has C_{2v} group symmetry with a planar geometry. The present calculations with B3LYP/TD-B3LYP, CCSD /EOM-CCSD, CASPT2, and CASSCF agree well with the experiment observation and the other

Table 1
The equilibrium geometries of ground state ($S_0(^1A_1)$), the first excited state ($S_1(^1B_1)$) and the second excited state ($S_2(^1B_2)$) of pyrimidine optimized by the present and other theoretical calculations in comparison with experimental data (bond distances in Å, angles and dihedral angles in degree and the atom numbering is shown in Fig. 1).

method	Sym	*r1*	*r2*	*r3*	*r4*	*r5*	*r6*	A1	A2	A3	A4	A5
					$S_0(^1A_1)$							
Exp.[66]	C_{2v}	1.328	1.350	1.393	1.082	1.079	1.087	128.0	116.0	121.2	117.8	120.9
Exp. [36,67]	C_{2v}	1.340	1.340	1.393	1.099	1.099	1.099	127.6	115.5	122.3	116.8	122.4
CAS(6,6)/ 6-311++g**	C_{2v}	1.328	1.329	1.391	1.074	1.076	1.074	126.5	116.6	121.8	116.6	121.4
CASSCF [56]	C_{2v}	1.337	1.332	1.392				127	116	122	117	
CCSD/CASPT2	C_{2v}	1.344	1.350	1.395	1.090	1.093	1.085	127.8	115.3	122.6	116.6	121.2
CCSD [54]	C_{2v}	1.346	1.346	1.402	1.091	1.092	1.089	127.6	115.5	122.4	116.5	121.2
CCSD [56]	C_{2v}	1.345	1.345	1.401				128	115	123	116	
					$S_1(^1B_1)$							
Calc.[55]	C_2	1.352	1.366	1.388	1.099	1.099	1.099	127.8	111.6	131.7	105.6	118.2
CCSD [54]	C_{2v}	1.327	1.395	1.403	1.088	1.087	1.091	118.0	123.6	118.4	117.8	124.2
CAS(6,6)/ 6-311++g**	C_{2v}	1.300	1.396	1.389	1.072	1.069	1.075	117.0	124.7	118.1	117.4	125.1
EOM-CCSD /CASPT2	C_{2v}	1.333	1.404	1.394	1.087	1.087	1.088	118.6	122.8	118.6	118.5	124.4
CASPT2 [56]	C_{2v}	1.331	1.400	1.404				119	123	119	118	
TD-B3LYP [56]	C_{2v}	1.322	1.390	1.394				118	123	119	118	
CASSCF [56]	C_{2v}	1.310	1.403	1.390				119	123	118	118	
EOM-CCSD [56]	C_{2v}	1.326	1.395	1.402				118	123	119	118	
CIS [56]	C_{2v}	1.306	1.363	1.383				116	125	118	118	
CIS [68]	C_{2v}	1.321	1.373	1.387	1.062	1.065		115.5	122.5	117.4	118.7	122.7
					$S_2(^1B_2)$							
CAS(6,6)/ 6-311++g**	C_{2v}	1.366	1.370	1.432	1.072	1.072	1.072	127.6	116.3	120.9	118.0	122.1
EOM-CCSD /CASPT2	C_{2v}	1.378	1.387	1.433	1.088	1.089	1.085	129.4	114.6	121.5	118.3	121.8
CASSCF [56]	C_{2v}	1.375	1.373	1.434				128	116	121	118	
EOM-CCSD [56]	C_{2v}	1.377	1.380	1.439				130	115	121	118	

theoretical simulations [54,56,66,67], except that the CASSCF results in which the C1–N9 bond (1.328 Å) is the same to the experimental results [66] but ca. 0.01 Å shorter than the other calculation results [54–56], while N9–C2 bond (1.329 Å) is close to Fischer et al.'s CASSCF result (1.332 Å) [56], however, both the present and the literature calculations are about 0.01 Å shorter than the experimental data [36,67]. Optimized equilibrium geometry parameters (bond distances and bond angles) of the three electronic states $S_0(^1A_1)$, $S_1(^1B_1)$, and $S_2(^1B_2)$ are shown in Table 1.

By studying the REMPI and MRTI spectroscopy plus theoretical simulation, Riese and Grotemeyer [68] suggested that the equilibrium geometry of the first excited state S_1 belongs to the C_{2v} group symmetry with a planar geometry, which is confirmed by Fischer et al.'s experimental and calculation results [56]. The present calculation did give the same results as the previous theoretical calculations for bond distances and bond angles within C_{2v} symmetry [54–56,68] at both CASSCF and EOM-CCSD levels, respectively. The present CASSCF calculations indicated that the first excited state is a $^1B_1$ symmetry with an excitation from molecular orbital B_2 to orbital A_2. This corresponds to an $n \rightarrow \pi^*$ transition and its molecular orbitals are shown in Fig. 3a as the pure excitation from HOMO → LUMO. This transition is interpreted as electronic transition from the lone-pair orbitals at the N atoms to the anti-π orbitals. As a consequence of the electronic transition, the ring –N– angle (C–N–C) rises by 8°, the angles N–C–N and N–C–C decrease by 10° and 4° respectively, the C2–N9 bond distance is elongated to 1.396 Å, and the C1–N9 bond decreases to 1.300 Å in the $S_1(^1B_1)$ state in comparison with ground state $S_0(^1A_1)$.

The second excited state $S_2(^1B_2)$ is also shown to be C_{2v} planar geometry. The present CASSCF and EOM-CCSD calculations proved that the second excited state is $^1B_2$ symmetry with an excitation from molecular orbital B_1 to orbital A_2, which is in agreement with

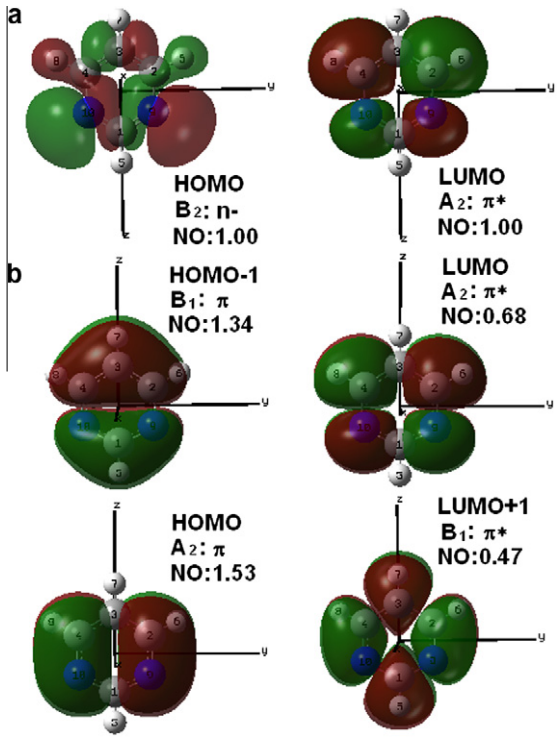

Fig. 3. Frontier molecular orbitals involved in (a) $S_0(^1A_1) \rightarrow S_1(^1B_1)$ and (b) $S_0(^1A_1) \rightarrow S_2(^1B_2)$ excitations.

Fischer's results [56]. This corresponds to $\pi \rightarrow \pi^*$ transition and its molecular orbitals are shown in Fig. 3b as the mixing excitation of the HOMO → LUMO + 1 and the HOMO − 1 → LUMO. This is in consistent with the literature [36,38,39]. In comparison to $S_0(^1A_1)$ geometry, the transition from π orbital to the anti-π orbital causes that all the bond distances in the ring and the C–H bonds elongate by 0.04 Å and reduce by 0.002 Å, respectively, while the bond angles N–C–N and C–C–C increase by 1°, and the angle C–N–C and N–C–C decreases by 1° at CASSCF level. In summary, all methods above are almost equally good for geometry optimizations and more critical comparison with experiment should be shown in spectral simulation.

3.2. Harmonic frequencies and anharmonic parameters

24-normal-mode harmonic frequencies for three electronic states $S_0(^1A_1)$, $S_1(^1B_1)$, and $S_2(^1B_2)$ are calculated using CAS(6,6)/6-311++g**, CASPT2/aug-cc-pVDZ, CCSD/EOM-CCSD/cc-pVDZ, B3LYP/TD-B3LYP/6-311++g** and methods, and only results from CAS and MP2 (for ground state) methods are shown in Table 2. In comparison with the Lord's [69] experimental results measured by the infra-red and Raman spectroscopy, both MP2 and CASSCF methods show good agreement with experiment (the MP2 method performs slightly better than the CASSCF method).

As analyzed in Section 2.1, the molecule structure changes due to the electronic transition from ground state to excited state, but what about change of corresponding frequencies. For nine total symmetry vibrational modes, the frequency differences between the excited states ($S_1(^1B_1)$ or $S_2(^1B_2)$) and the ground state ($S_0(^1A_1)$) are considerably small (see in Table 2). Therefore, the displaced oscillator approximation can be considered as a good approximation for simulating electronic spectroscopy. The Huang–Rhys factor in Eq. (6) and the displacement (d_j) in Eq. (7) were estimated for the first and second excited states respectively as shown in Table 2. Five modes ν_{6a}, ν_1, ν_{12}, ν_{13}, and ν_2 are shown significant figures for the first excited state and four modes ν_{6a}, ν_1, ν_{12}, and ν_2 for the second excited state. This agrees well with explanations that the great changes in the inner angles of the ring account for the highest intensity of the bending mode 6a (see Fig. 4) in the vibronic spectrum, and the variations of bond lengths in the ring are responsible for valence bending modes 1 and 12 (see Fig. 4) in the vibronic spectrum [55]. Both CASSCF and MP2 methods produce satisfactory predictions for the most contributing modes in the present spectrum simulation.

Table 2
Experimental (exp) and calculated (MP2, CAS/s0) vibrational frequencies (cm^{-1}) for ground state, and the calculated frequencies differences between $S_1(^1B_1)$ and $S_0(^1A_1)$ states (s1–s0), and between $S_2(^1B_2)$ and $S_0(^1A_1)$ states (s2–s0). Calculated Huang–Rhys factors (S(s1) and S(s2)), displacements (d(s1) and d(s2), in atomic units) and anharmonic parameters (an(s1) and an(s2)) for $S_1(^1B_1)$ and $S_2(^1B_2)$.

Vibration normal modes [36,69]			$S_0(^1A_1)$		$S_1(^1B_1)$				$S_2(^1B_2)$			
Sym	N_0	Mode	Exp. [36]	CAS(MP2)	s1–s0	S(s1)	d(s1)	an(s1)	s2–s0	S(s2)	d(s2)	an(s2)
A_1	6a	Cp	677	734(687)	−38	1.566	−0.265	−0.004	−72	0.044	0.044	0.001
	1	CC	991	1068(1010)	−80	0.299	0.089	−0.035	−85	1.402	0.193	−0.077
	12	Cp	1065	1135(1076)	−41	0.454	0.160	−0.043	−130	0.153	0.093	−0.025
	9a	Hp	1147	1218(1158)	−31	0.048	−0.059	−0.007	−93	0.020	−0.038	−0.005
	19a	CC	1398	1527(1437)	17	0.012	−0.030	0.001	−98	0.002	0.012	−0.000
	8a	CC	1570	1715(1609)	−79	0.086	0.053	−0.019	−81	0.000	−0.002	0.001
	20a	CH	3038	3326(3200)	12	0.000	−0.002	0.003	32	0.090	0.077	−0.097
	13	CH	3052	3352(3218)	34	0.319	−0.145	−0.300	23	0.014	−0.031	−0.064
	2	CH	3074	3361(3243)	41	0.188	0.111	−0.206	22	0.120	0.089	−0.165
A_2	16a	Co	399	444(386)	−193	0.000	0.000	0.000	−170	0.000	0.000	0.000
	17a	Ho	927	1012(919)	−546	0.000	0.000	0.000	−406	0.000	0.000	0.000
B_1	16b	Co	344	408(299)	−48	0.000	0.000	0.000	−124	0.000	0.000	0.000
	4	Co	721	752(674)	−282	0.000	0.000	0.000	−264	0.000	0.000	0.000
	10b	Ho	811	840(776)	−212	0.000	0.000	0.000	−250	0.000	0.000	0.000
	17b	Ho	955	990(880)	−59	0.000	0.000	0.000	−299	0.000	0.000	0.000
	5	Ho	980	1028(928)	21	0.000	0.000	0.000	−284	0.000	0.000	0.000
B_2	6b	Cp	623	670(625)	−28	0.000	0.000	0.000	−94	0.000	0.000	0.000
	18b	Hp	1071	1081(1092)	−115	0.000	0.000	0.000	−95	0.000	0.000	0.000
	15	Hp	1159	1164(1243)	−112	0.000	0.000	0.000	91	0.000	0.000	0.000
	14	CC	1225	1318(1321)	50	0.000	0.000	0.000	141	0.000	0.000	0.000
	3	Hp	1370	1494(1398)	−66	0.000	0.000	0.000	25	0.000	0.000	0.000
	19b	CC	1466	1602(1492)	−115	0.000	0.000	0.000	33	0.000	0.000	0.000
	8b	CC	1568	1718(1616)	−182	0.000	0.000	0.000	168	0.000	0.000	0.016
	7b	CH	3086	3332(3205)	61	0.000	0.000	0.000	38	0.000	0.000	0.000

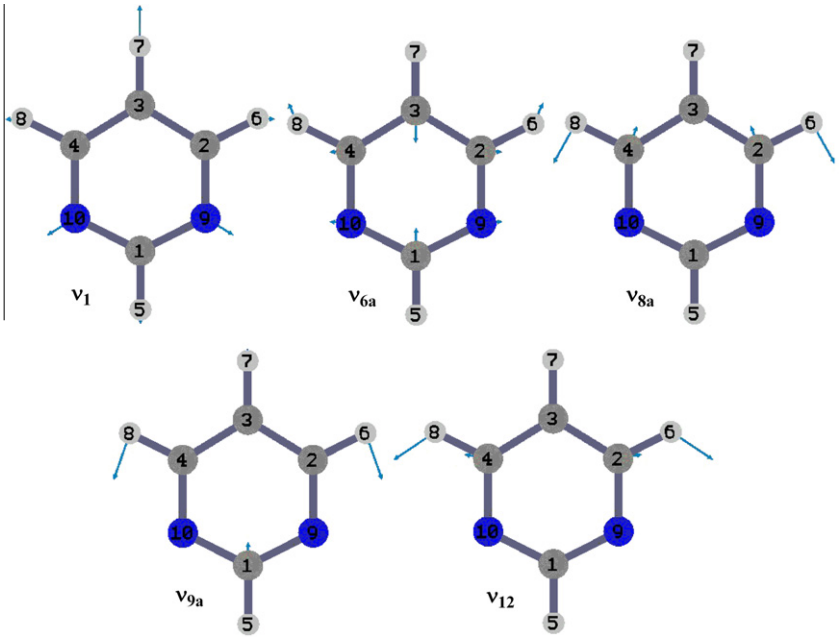

Fig. 4. Five main vibrational modes calculated at CASSCF(6,6)/6-311++G** level.

Table 3
Calculated and observed vertical excitation energies (in eV) and its discrepancies Δ between theory and experiment with corresponding oscillator strengths f for $^1B_1$ and $^1B_2$ transitions.

Method	$^1B_1$	$\Delta(1)$	$f(1)$	$^1B_2$	$\Delta(2)$	$f(2)$
Exp. (max) [38,39,56]	4.20		0.007[36]	5.20		0.05 [36]/0.028 [53]
Exp. (max-new) [49]	4.183			5.22		
Exp. (ZPE corrected) [52]	4.3			5.3		
CASPT2 [56,70]	3.81	−0.39		4.93	−0.27	
TD-B3LYP [56]	4.31	0.11		5.87	0.67	
TD-B3LYP	4.26	0.06		5.77	0.57	
EOM-CCSD	4.62	0.42	0.0063	5.58	0.38	0.0303
EOM-CCSD [56]	4.74	0.54		5.52	0.32	
EOM-CCSD(T) [52]	4.24	0.04		5.01	−0.19	
STEOM-CCSD [53,56]	4.40	0.20		5.04	−0.16	
CCSD R(3) [54]	4.55	0.35		5.44	0.24	
SAC-CI SD-R [51]	4.32	0.12	0.0063	5.29	0.09	0.0327

Table 4
Calculated and observed adiabatic excitation energies (E_{ad}, in eV) and its discrepancies Δ between theory and experiment for S_1 and S_2 states.

Method	$E_{ad}(S_1)$	$\Delta(1)$	$E_{ad}(S_2)$	$\Delta(2)$
Exp. (0–0-old assn.)	3.85 [36,38,39,50]		5.00 [36,38,39]	
Exp. (0–0-new assn.) [49]	3.854		5.01(6)	
CASPT2//CAS(6,6)	3.51	−0.34	5.01	0.01
EOM-CCSD/aug-cc-pVDZ	3.56	−0.29	5.17	0.17
TD-B3LYP	3.84	−0.01	5.59	0.59
CASPT2//CASSCF(18,12)/6-31 + G*[76]	3.75	−0.10		
EOM-CCSD/6-31 + G* [76]	4.28	0.43		
EOM-CCSD [56]	4.17	0.32	5.29	0.29
TD-B3LYP/6-31 + G* [76]	3.88	0.03		
CCS/cc-pVDZ [54]	5.44	1.59	6.62	1.62
CCSD/DZPR [54]	4.26	0.41	5.26	0.26
CIS [56]	5.32	1.47	6.48	1.48

Following the conventional scheme for the assignment of the vibrational normal modes [69], we found that there are the following typical vibrational modes as CC carbon–carbon stretching, CH carbon–hydrogen stretching, Cp in-plane ring bend, Co out of plane ring bend, Hp in-plane CH bending, and Ho out of plane CH bending. The corresponding modes are given in Table 2. For example, the A_1 symmetry mode with Huang–Rhys factor 1.566 for $S_1(^1B_1)$ excited state corresponds to the vibration mode of 734 cm^{-1} in the CASSCF method, which can be assigned as ν_{6a} mode, namely a in plane-ring bend mode (Cp).

The cubic force constants (K_{j3} in Eq. (9)) were calculated by MP2/6-311++g** method and then they were converted into

anharmonic parameters η_j by Eq. (10) as shown in Table 2. Except for modes ν_{13} and ν_2, anharmonic parameters η_j are generally small.

3.3. Vertical, adiabatic excitation energies

We calculated the vertical excitation energies as shown in Table 3 and adiabatic excitation energies as shown in Table 4. Combined the present calculations and the literature results [51–54,56,70,76], most of the methods overestimate the excitation energies, except that the present TD-B3LYP calculation shows the best agreement with the experimental observations for both vertical and adiabatic excitation energies of the first excited $S_1(^1B_1)$ state, and the SAC-CISD-R [51] and the present CASPT2//CAS(6,6) calculations show the best agreement with the experimental observations for vertical and adiabatic excitation energies of the second excited $S_2(^1B_2)$ state, respectively (see in Tables 3 and 4). Conventionally, computational studies of pyrimidine [51–53,56,57,70–75] focused mainly on the evaluation of vertical excitation energies and oscillator strength with the aims of spectral assignment. For the vertical excitation from ground state to the first excited state, experimental spectrum predicted the peak of the band maximum is located at 4.20 eV [38,39,56] with the zero-point energy correction up to 4.30 eV [52]. For the vertical excitation from ground state to the second excited state, the experiment predicated the peak of the band maximum is located at 5.20 eV [38,39,56] with the zero-point energy correction up to 5.30 eV [52]. Regarding to oscillator strengths of the excitation as shown in Table 3, both EOM-CCSD and SAC-CI [51] methods show good agreement with experiment. The experiment shows that the oscillator strength of $n \rightarrow \pi^*$ transition is about a quarter of that of $\pi \rightarrow \pi^*$ transition. Thus it leads to that the $^1B_1$ band intensity is much smaller than $^1B_2$.

Although the calculations of vertical excitation energies and the oscillator strengths can qualitatively describe the peaks of the band maximum and the relative intensity for the spectra, this is not an entirely correct assumption (it may include errors of some tenths of an eV). For example, they cannot consider the origin bands for transitions in which the electronic transition causes a significant change in molecular geometry. A way to unequivocally compare equivalent quantities between theory and experiment is to compare 0–0 transition energies [51].

In the present study, simulations of vibronic spectra were based on the adiabatic excitation energies appeared in Eqs. (2) and (3) in which $\omega_{ab} + \Omega_0$ that includes Ω_0 as a dynamic effect of vibronic spectra should correspond to observed 0–0 excitation energy in experiment. The present work shows that this dynamic effect comes from the first-order anharmonic correction. When we simulate vibronic spectra with one method, we choose the corresponding adiabatic excitation energy of this method in Table 4. It should be noted that in the single vibronic manifold spectra the adiabatic excitation energies do not influence the band shape of spectra.

We utilized CSSCF/CSPT2 method to calculate conical intersection (CI) between S_1 and S_2 states, and we found that the geometry of CI is close to S_1 state and the energy of CI is higher than the minimum energy of S_2 state. The present analytical formulation of anharmonic Franck–Condon factor in Eqs. (2) and (3) can be valid for vibronic spectra with low vibrational number, so that this CI is not needed to be included in the present simulation. However, this CI confirms that anharmonic effect for S_1 state can be large as its geometry close to S_1 state.

3.4. Analysis of distorted effects and calculation of reorganization energies

We have analyzed the total symmetric vibrational modes with Huang–Rhys factors, and they play dominant roles in the progressions of the absorption [49,56] and fluorescence [50] spectra of the S_1 state. There are few overtones of out-of-plane vibrations were described and interpreted as contribution from the non-totally symmetric vibrational modes in the experimental spectra [49,50]. For example, the transition $16a^2$ with a_2 symmetry has relative strong/weak intensity in the absorption/fluorescence spectrum and this is not included in the simulation with displaced harmonic oscillator approximation. We implement the distorted harmonic oscillator approximation [77] to analyze non-totally symmetry modes in comparison with total symmetric vibrational modes. As

Table 5
The calculated Franck–Condon factors in the displaced harmonic approximation (FC_{disp}) and the distorted harmonic approximation (FC_{dist}).

C_{2v} species	Vibration normal modes		cas/s0	cas/s1	FC_{disp}	FC_{dist}
A_1	6a	Cp	734	696	0.3271	0.0000
	1	CC	1068	988	0.2220	0.0000
	12	Cp	1135	1094	0.2882	0.0000
	9a	Hp	1218	1187	0.0457	0.0000
	19a	CC	1527	1544	0.0124	0.0000
	8a	CC	1715	1636	0.0791	0.0000
	20a	CH	3326	3338	0.0001	0.0000
	13	CH	3352	3386	0.2321	0.0000
	2	CH	3361	3402	0.1557	0.0000
A_2	16a	Co	444	251	0.0000	0.0371
	17a	Ho	1012	466	0.0000	0.0635
B1	16b	Co	408	360	0.0000	0.0020
	4	Co	752	470	0.0000	0.0258
	10b	Ho	840	628	0.0000	0.0103
	17b	Ho	990	931	0.0000	0.0005
	5	Ho	1028	1049	0.0000	0.0000
B2	6b	Cp	670	642	0.0000	0.0002
	18b	Hp	1081	966	0.0000	0.0016
	15	Hp	1164	1052	0.0000	0.0013
	14	CC	1318	1368	0.0000	0.0002
	3	Hp	1494	1428	0.0000	0.0002
	19b	CC	1602	1487	0.0000	0.0007
	8b	CC	1719	1537	0.0000	0.0016
	7b	CH	3332	3393	0.0000	0.0000

Table 6
Calculated reorganization energy (eV) for ground state ($\lambda_0(S_1)$, $\lambda_0(S_2)$), excited $S_1(^1B_1)$ state ($\lambda_{ex}(S_1)$), and excited $S_2(^1B_2)$ state ($\lambda_{ex}(S_2)$).

Vibration normal modes [36,69]			$S_0(^1A_1)$	$S_1(^1B_1)$		$S_2(^1B_2)$	
Sym	N_0	Mode	CAS(MP2)	$\lambda_0(S_1)$	$\lambda_{ex}(S_1)$	$\lambda_0(S_2)$	$\lambda_{ex}(S_2)$
A_1	6a	Cp	734(687)	0.13	0.13	0.00	0.00
	1	CC	1068(1010)	0.04	0.04	0.19	0.16
	12	Cp	1135(1076)	0.06	0.06	0.02	0.02
	9a	Hp	1218(1158)	0.01	0.01	0.00	0.00
	19a	CC	1527(1437)	0.00	0.00	0.00	0.00
	8a	CC	1715(1609)	0.02	0.02	0.00	0.00
	20a	CH	3326(3200)	0.00	0.00	0.04	0.03
	13	CH	3352(3218)	0.16	0.09	0.01	0.01
	2	CH	3361(3243)	0.09	0.06	0.06	0.04
Total λ with anharmonic correction				0.51	0.41	0.32	0.27
Total λ from the PES				0.68	0.59	0.26	0.26

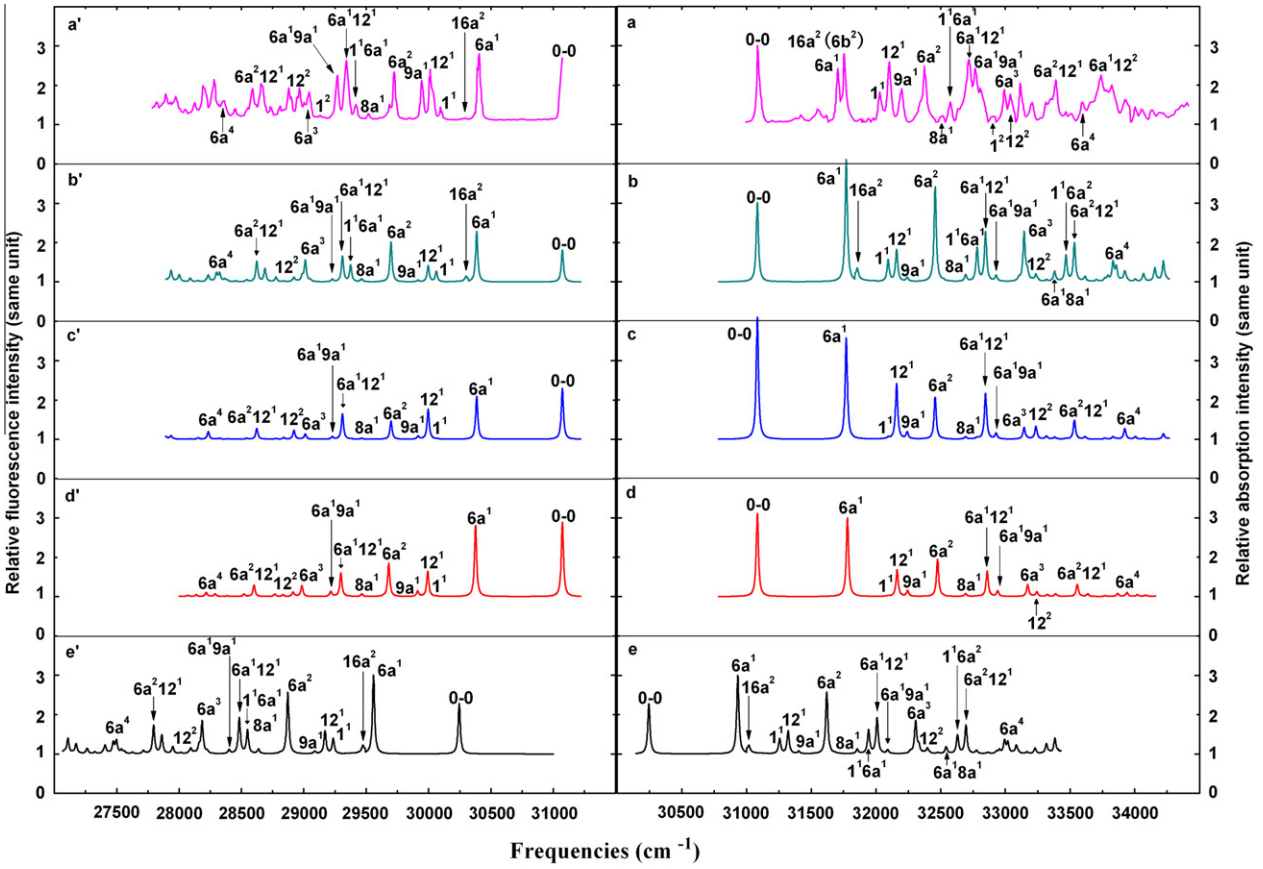

Fig. 5. $S_1(^1B_1) \leftarrow S_0(^1A_1)$ absorption spectrum and $S_1(^1B_1) \rightarrow S_0(^1A_1)$ fluorescence spectrum of pyrimidine. Respectively, experimental data from (a) Ref. [49], [56] and (a′) Ref. [50]; Simulated results with the present anharmonic correction, (b) and (b′) CASSCF, (c) and (c′) EOM-CCSD, (d) and (d′) TD-B3LYP; Simulated results with the present harmonic oscillator approximation (e) and (e′) CASSCF.

shown in Table 2, some of the out-of-plane vibrations have a large change in frequencies. For example, for the mode ν_{16a} with a_2 symmetry, the frequency difference between S_0 and S_1 states is 193 cm^{-1} and in this case the distorted effect might be important.

Within displaced approximation, Franck–Condon factor can be derived as [24,77]

$$F_{v_i'} = \left|\left\langle \Theta_{bv_i'} | \Theta_{a0_i} \right\rangle\right|^2 = \frac{S_i^{v_i'}}{v_i'!} e^{-S_i} \tag{14}$$

where v_i' denotes the vibrational quantum number of the ith normal mode and S_i is the Huang–Rhys factor. Similarly, the Franck–Condon factor in the distorted harmonic approximation is given by [24,77]

$$F_{v_i'} = \left|\left\langle \Theta_{bv_i'} | \Theta_{a0_i} \right\rangle\right|^2 = \frac{\sqrt{\omega_i \omega_i'}}{\omega_i + \omega_i'} \left(\frac{\omega_i' - \omega_i}{\omega_i' + \omega_i}\right)^{v_i'} \frac{v_i'!}{2^{v_i'-1}[(v_i'/2)!]^2} \tag{15}$$

where v_i' can be only taken as an even integer number, ω_i and ω_i' correspond to vibrational frequencies for different electronic states. We can see that, unless$\omega_i' \gg \omega_i$ (or $\omega_i' \ll \omega_i$), $F_{v_i'}$ is much smaller than unity. By applying Eqs. (14) and (15), we have computed the displaced Franck–Condon factors of 0–1 transitions and the distorted ones of 0–2 bands for all 24 vibrational modes and their values are listed in Table 5. Obviously, the intensities of 0–2 transitions (overtones) of the out-of-plane modes are very small in comparison with 0–1 transitions (for example, the largest Franck–Condon factor arises from transition of $16a^2$ is only 0.0371 based on the CASSCF

calculation). Therefore, we conclude that distorted effect is small in vibronic spectra of pyrimidine.

We calculated the reorganization energy using Eqs. (12) and (13) for S_0, S_1 and S_2 states within the first-order anharmonic correction and results are summarized in Table 6 in which the reorganization energy contributed from each mode is also listed. A reorganization energy difference between the ground and the first excited state calculated from the first-order correction agrees with exact value 0.11 eV. However, this difference between the ground and the second excited state is about 0.05 eV (exact value is zero in Table 6). If we include the distorted contribution, the difference becomes 0.03 eV for the second excited state. Then, we conclude that the first-order correction to reorganization energy is significant to S_1 and negligible to S_2 state. This agrees with conclusion for spectral simulation in next subsection.

3.5. Anharmonic and harmonic Franck–Condon simulations

The present MP2 frequencies in Table 2 are actually utilized in the simulation of both absorption and fluorescence spectra for the two excited states within displaced harmonic and anharmonic oscillator approximations for CASSCF and EOM-CCSD methods, while the B3LYP frequencies is adopted for the TD-B3LYP method. The dephasing constants γ_{ba} in Eqs. (2) and (3) are chosen as 10 cm^{-1} and 700 cm^{-1} for the excited states $S_1(^1B_1)$ and $S_2(^1B_2)$, respectively. This choice includes resolution broadening in the experiment and it is similar to that of Refs. [41,44,45]. Temperature is taken as 298 K in the simulation as the experimental spectra were measured at room temperature. The intensity of simulated absorption and fluorescence spectra is in the same unit for S_1 state as shown in Fig. 5.

Fig. 5 shows that the main progressions of vibronic bands for the S_1 absorption and fluorescence spectra that are well described by mode ν_{6a} accompanied with modes ν_1 and ν_{12}. In fact, this can be easily understood from that the Huang–Rhys factors for the modes ν_{6a}, ν_1, and ν_{12} are 1.566, 0.299, and 0.454 (see Table 2), respectively. The overall agreement between experimental (shown in Fig. 5a [49,56] and Fig. 5a′ [50]) and the presently simulated spectra is generally good. However, the highest peak is assigned as the 0–0 vibronic transition for the absorption and the $6a_0^1$ transition for fluorescence spectra from experimental, while the $6a_0^1$ is the strongest transition for both the absorption and fluorescence spectra from the present harmonic calculation. When the anharmonic quantity $\eta_{6a} = -0.004$ (see Table 2) is included and this makes effective the Huang–Rhys factor for absorption as $S'_{6a} = S_{6a}(1 + 3\eta_{6a}) = 1.547$ and for fluorescence as $S'_{6a} = S_{6a}(1-3\eta_{6a}) = 1.585$, the ν_{6a} transition profiles and relative intensity changes in the right direction as illustrated in Fig. 5b and b′. Fig. 5e and e′ shows that the peak position of the 0–0 excitation from harmonic oscillator approximation has a big discrepancy with experiment observation for both absorption and fluorescence spectra although the best static excitation energy $|\omega_{ab}| = 3.75$ eV (see Table 4) is chosen for simulation of the S_1 state. When anharmonic corrections are included in the simulation, Fig. 5b and b′ shows that the peak position of the 0–0 excitation has blue shift $\Omega_0 = 827$ cm^{-1} with respect to harmonic oscillator approximation and this leads to a very good agreement with experimental observation. Actually, this dynamic shift was obtained with scaling factor 0.8745 to all anharmonic constants η_j in Table 2. This kind scaling is widely employed for vibrational frequencies and we think that it is in the same reason to scaling anharmonic constants. We conclude that the first-order anharmonic correction makes spectral peak positions shift and intensities change in the right direction simultaneously for absorption and fluorescence spectra of S_1 state; enhanced intensity of the absorption spectra and weakened intensity of the fluorescence. Finally, we have included the distorted effect for the non-total symmetric mode $16a^2$ as is shown in Fig. 5b, e, b′ and e′ for a very weak band, which agrees very well with Knight's experimental results. Furthermore, the present EOM-CCSD and TD-B3LYP spectral simulations with anharmonic corrections are similar to the CASSCF simulation, except the highest peak for both absorption and fluorescence of S_1 state now is 0–0 vibronic transition, but the intensity of the weak band is much weaker than that of CASSCF and experiment. We can see that the simulated fluorescence spectrum of S_1 state show better agreement with the experimental results than the simulated absorption spectrum. The discrepancy may be because that the strong experimental absorption spectrum of S_2 state affects the absorption spectrum of S_1 state, while the weak fluorescence spectrum of S_2 state has little effects to the strong fluorescence spectrum of S_1 state during the experiment.

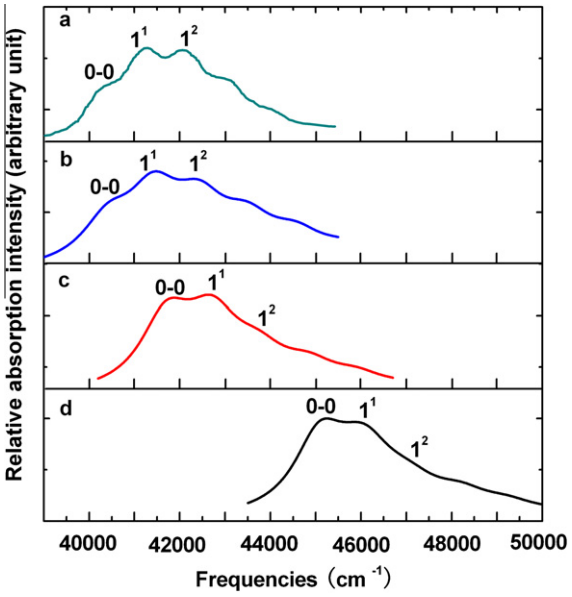

Fig. 6. $S_2(^1B_2) \leftarrow S_0(^1A_1)$ absorption spectrum of pyrimidine simulated results with the present harmonic oscillator approximation. (a) Experimental data from Ref. [38], (b) CASSCF, (c) EOM-CCSD and (d) TD-B3LYP.

The largest Huang–Rhys factor for the $S_2(^1B_2)$ state listed in Table 2 is 1.402 for vibrational mode ν_1 accompanied by the other two; 0.044 for the mode ν_{6a} and 0.153 for mode ν_{12}. Fig. 6b shows simulated absorption spectrum of the $S_2(^1B_2)$ state with the displaced harmonic oscillator approximation at CASSCF level, and 1_0^1 is shown to be the strongest vibronic transition which agrees well with the experimental spectra [49]. Fig. 6b shows that the both spectral peak position and the profile is in very good agreement with experimental result. Anharmonic correction to the absorption spectrum of the $S_2(^1B_2)$ is negligible in the present simulation. In addition, Fig. 6c and d show the EOM-CCSD and TD-B3LYP simulated spectral profiles which are similar to Fig. 6b. Compare to the strongest vibronic transition 1_0^1, the 0–0 band intensity from EOM-CCSD simulation is stronger than that of the CASSCF simulation and the experiment. However, the highest peak is assigned as the 0–0 vibronic transition for the TD-B3LYP simulation.

4. Concluding remarks

We have simulated absorption and fluorescence spectra for $S_1(^1B_1)$ state and the absorption spectrum for $S_2(^1B_2)$ state using harmonic and anharmonic oscillator approximation for pyrimidine molecule. We found that the first-order anharmonic correction makes a significant contribution to band shift of spectra for S_1 state but it has no meaningful contribution to S_2 state. Franck–Condon

simulations with including the first-order anharmonic correction show intensity enhancement of the absorption and intensity weakening of fluorescence for the adiabatic $S_1(^1B_1)$ state and this agrees well with experimental observation. Franck–Condon simulation of the absorption spectrum for the adiabatic $S_2(^1B_2)$ state shows good agreement with experimental observation without the anharmonic correction.

We have optimized the equilibrium geometries of the electronic ground and the two lowest singlet excited states and then computed their 24-normal-mode frequencies that are all positive. All three electronic states have C_{2v} group symmetry. We confirmed that our calculation results are basically the same as those from high-level ab initio calculation in the literatures [54–56]. This means that the equilibrium geometries from the present calculation are accurate enough to be used for spectrum simulation.

The electronic structure calculations confirmed that the $S_1(^1B_1)$ and $S_2(^1B_2)$ states have $n\pi^*$ and $\pi\pi^*$ configurations, respectively. Both vertical and adiabatic excitation energies of the $S_1(^1B_1)$ and $S_2(^1B_2)$ states are calculated and analyzed by comparing with various theoretical calculations and experimental results. Basically, even the best calculations for static adiabatic excitation energies of the $S_1(^1B_1)$ state differ from the experimental one, and the best calculation for static adiabatic excitation energy of $S_2(^1B_2)$ state agree exactly with the experimental one. This reflects that dynamic shift of excitation energies from anharmonic correction is significant for the $S_1(^1B_1)$ state, but not for $S_2(^1B_2)$ state. This is same as reorganization energy calculations that confirm 0.1 eV discrepancy between $\lambda_0(S_1)$ and $\lambda_{ex}(S_1)$ but little discrepancy between $\lambda_0(S_2)$ and $\lambda_{ex}(S_2)$.

The present studies indicate that the frequency for each of the nine total symmetric normal modes only slightly differs from one another for the three electronic states $S_0(^1A_1)$, $S_1(^1B_1)$ and $S_2(^1B_2)$. Furthermore, the transformation matrices that transfer geometric structure configuration from Jacobi to normal-mode coordinates for the three electronic states are also quite same for each of the nine total symmetric modes. Thus, displaced harmonic oscillator approximation is proved to be good approximation. In fact, Huang–Rhys factors directly indicate that the modes ν_{6a}, ν_1, and ν_{12} contribute S_1 absorption and fluorescence spectra, and S_2 absorption spectrum mostly, among which the main progression of S_1 bands comes from mode ν_{6a} and S_2 bands comes from mode ν_1. This agrees with experimental measurement [49]. Although all ab initio CASSCF, CSPT2, CCSD/EOM-CCD and B3LYP/TD-B3LYP methods basically show good agreement with experimental results for vibronic spectra of pyrimidine molecule, the CASSCF shows the best agreement with experiment for weak-band intensities of vibronic spectra. This is because that CASSCF method provides equal footing calculation for electronic and excited states, and thus it produces the most accurate results for geometry differences between the ground and excited states. It should be emphasized that vibronic spectra is the most sensitive to the geometry difference, not absolute geometry for particular electronic state.

The non-total symmetric vibrational mode 16a is taken into account in the present spectrum simulation within the distorted harmonic approximation and it devotes a weak band $16a^2$. The other non-total symmetric modes are negligible in spectrum simulation. The present first-order anharmonic corrections can only take into account diagonal part of anharmonicity so that it is not enough to correct detailed band shape in vibronic spectra. This is because that mode mixings due to off-diagonal part of anharmonicity are completely neglected as they belong to the second-order anharmonic corrections along with Duschinsky mode mixings. The conventional Herzberg–Teller effect of intensity borrowing from the other nontotally symmetric vibrational modes and possible nonadiabatic coupling due to conical intersection are not considered in the present studies as they both have little effect to totally symmetric vibrational modes.

Acknowledgments

L.Y. thanks support from visiting graduate program in National Chiao-Tung University. This work is supported by National Science Council of the Republic of China under Grant Nos. 97-2113-M-009-010-MY3 and 100-2113-M-009-005-MY3. J.Y. would like to thank support from National Natural Science Foundation of People's Republic of China under Grant Nos. 20733002, 20873008, and 21073014. C.Z. thanks the MOE-ATU project of the National Chiao Tung University for support.

References

[1] J. Franck, Trans. Faraday Soc. 21 (1925) 536.
[2] E.U. Condon, Phys. Rev. 28 (1926) 1182.
[3] E.U. Condon, Phys. Rev. 32 (1928) 872.
[4] F. Duschinsky, Acta Physicochim. URSS 7 (1937) 551.
[5] T.E. Sharp, H.M. Rosenstock, J. Chem. Phys. 41 (1964) 3453.
[6] S.H. Lin, J. Chem. Phys. 44 (1966) 3759.
[7] S.H. Lin, R. Bersohn, J. Chem. Phys. 44 (1966) 3768.
[8] S.H. Lin, J. Chem. Phys. 58 (1973) 5760.
[9] L.S. Cederbaum, W. Domcke, J. Chem. Phys. 64 (1976) 603.
[10] E.V. Doktorov, I.A. Malkin, V.I. Manko, J. Mol. Spectrosc. 64 (1977) 302.
[11] M.J.S. Dewar, E.G. Zoebisch, E.F. Healy, J.J.P. Stewart, J. Am. Chem. Soc. 107 (1985) 3902.
[12] M. Roche, Chem. Phys. Lett. 168 (1990) 556.
[13] S.Y. Lee, J. Phys. Chem. – US 9 (4) (1990) 4420.
[14] D.C. Todd, G.R. Fleming, J.M. Jean, J. Chem. Phys. 97 (1992) 8915.
[15] F. Zerbetto, J. Phys. Chem. – US 9 (8) (1994) 13157.
[16] P.T. Ruhoff, Chem. Phys. 186 (1994) 355.
[17] P.A. Malmqvist, N. Forsberg, Chem. Phys. 228 (1998) 227.
[18] T. Muller, P.H. Vaccaro, F. Perez-Bernal, F. Iachello, J. Chem. Phys. 111 (1999) 5038.
[19] D.K.W. Mok, E.P.F. Lee, F.T. Chau, D.C. Wang, J.M. Dyke, J. Chem. Phys. 113 (2000) 5791.
[20] P.T. Ruhoff, M.A. Ratner, Int. J. Quant. Chem. 77 (2000) 383.
[21] S. Schumm, M. Gerhards, K. Kleinermanns, J. Phys. Chem. A 104 (2000) 10648.
[22] J.R. Reimers, J. Chem. Phys. 115 (2001) 9103.
[23] V. Zazubovich, I. Tibe, G.J. Small, J. Phys. Chem. B 105 (2001) 12410.
[24] S.H. Lin, C.H. Chang, K.K. Liang, R. Chang, Y.J. Shiu, J.M. Zhang, T.S. Yang, M. Hayashi, F.C. Hsu, Adv. Chem. Phys. 121 (2002) 1.
[25] H. Kikuchi, M. Kubo, N. Watanabe, H. Suzuki, J. Chem. Phys. 119 (2003) 729.
[26] H. Hwang, P.J. Rossky, J. Phys. Chem. A 108 (2004) 2607.
[27] J.M. Luis, D.M. Bishop, B. Kirtman, J. Chem. Phys. 120 (2004) 813.
[28] A. Hazra, H.H. Chang, M. Nooijen, J. Chem. Phys. 121 (2004) 2125.
[29] M. Dierksen, S. Grimme, J. Phys. Chem. A 108 (2004) 10225.
[30] M. Dierksen, S. Grimme, J. Chem. Phys. 122 (2005) 244101.
[31] S. Yeganeh, M.A. Ratner, J. Chem. Phys. 124 (2006) 044108.
[32] I. Pugliesi, K. Muller-Dethlefs, J. Phys. Chem. A 110 (2006) 4657.
[33] I. Pugliesi, K. Muller-Dethlefs, J. Phys. Chem. A 110 (2006) 13045.
[34] T. Petrenko, O. Krylova, F. Neese, M. Sokolowski, New J. Phys. 11 (2009) 015001.
[35] C.Y. Zhu, K.K. Liang, M. Hayashi, S.H. Lin, Chem. Phys. 358 (2009) 137.
[36] (a) K.K. Innes, J.P. Byrne, I.G. Ross, J. Mol. Spectrosc. 22 (1967) 125; (b) K.K. Innes, I.G. Ross, W.R. Moomaw, J. Mol. Spectrosc. 132 (1988) 492.
[37] A.D. Boese, J.M.L. Martin, J. Phys. Chem. A 108 (2004) 3085.
[38] A. Bolovinos, P. Tsekeris, J. Philis, E. Pantos, G. Andritsopoulos, J. Mol. Spectrosc. 103 (1984) 240.
[39] I. Yamazaki, T. Murao, T. Yamanaka, K. Yoshihara, Faraday Discuss. Chem. Soc. 75 (1983) 395.
[40] M. Chachisvilis, A.H. Zewail, J. Phys. Chem. A 103 (1999) 7408.
[41] Z.-L. Cai, J.R. Reimers, J. Phys. Chem. A 104 (2000) 8389.
[42] P. Wormell, J.E. Gready, Chem. Phys. 179 (1994) 55.
[43] P.L. Muiño, P.R. Callis, J. Chem. Phys. 100 (1994) 4093.
[44] H. Wang, C. Zhu, J.-G. Yu, S.H. Lin, J. Phys. Chem. A 113 (2009) 14407.
[45] D.-Y. Wu, M. Hayashi, Y.J. Shiu, K.K. Liang, C.H. Chang, S.H. Lin, J. Chin. Chem. Soc. 50 (2003) 735.
[46] R. He, C. Zhu, C.-H. Chin, S.H. Lin, Sci. China Ser. B – Chem. 51 (2008) 1166.
[47] R. He, C. Zhu, C.-H. Chin, S.H. Lin, Chem. Phys. Lett. 476 (2009) 19.
[48] M.H. Palmer, I.C. Walker, M.F. Guest, A. Hopkirk, Chem. Phys. 147 (1990) 19.
[49] F. Ferreira da Silva, D. Almeida, G. Martins, A.R. Milosavljević, B.P. Marinković, S.V. Hoffmann, N.J. Mason, Y. Nunes, G. Garcia, P. Limão-Vieira, Phys. Chem. Chem. Phys. 12 (2010) 6717.
[50] A.E.W. Knight, C.M. Lawburgh, C.S. Parmenter, J. Chem. Phys. 63 (1975) 4336.
[51] Y. Li, J. Wan, X. Xu, J. Comput. Chem. 28 (2007) 1658.
[52] J.E. Del Bene, J.D. Watts, R.J. Bartlett, J. Chem. Phys. 106 (1997) 6051.
[53] M. Nooijen, Spectrochim. Acta Part A 55 (1999) 539.

[54] A. Öhrn, O. Christiansen, Phys. Chem. Chem. Phys. 3 (2001) 730.
[55] K.V. Berezin, L.M. Babkov, M.A. Kovner, J. Struct. Chem. 38 (1997) 281.
[56] G. Fischer, Z.-L. Cai, J.R. Reimers, P. Wormell, J. Phys. Chem. A 107 (2003) 3093.
[57] P.-A. Malmqvist, B.O. Roos, M.P. Fülscher, A.P. Rendell, Chem. Phys. 162 (1992) 359.
[58] F. Billes, H. Mikosch, S. Holly, J. Mol. Struct. (THEOCHEM) 423 (1998) 225.
[59] Y. Luo, H. Ågren, S. Knuts, P. Jørgensen, Chem. Phys. Lett. 213 (1993) 356.
[60] L. Åsbrink, C. Fridh, B.Ö. Jonsson, E. Lindholm, Int. J. Mass Spectrom. Ion Phys. 8 (1972) 215.
[61] M.J. Frisch, G.W. Trucks, H.B. Schlegel, G.E. Scuseria, M.A. Robb, J.R. Cheeseman, J.A. Montgomery Jr., T. Vreven, K.N. Kudin, J.C. Burant, J.M. Millam, S.S. Iyengar, J. Tomasi, V. Barone, B. Mennucci, M. Cossi, G. Scalmani, N. Rega, G.A. Petersson, H. Nakatsuji, M. Hada, M. Ehara, K. Toyota, R. Fukuda, J. Hasegawa, M. Ishida, T. Nakajima, Y. Honda, O. Kitao, H. Nakai, M. Klene, X. Li, J.E. Knox, H.P. Hratchian, J.B. Cross, V. Bakken, C. Adamo, J. Jaramillo, R. Gomperts, R.E. Stratmann, O. Yazyev, A.J. Austin, R. Cammi, C. Pomelli, J.W. Ochterski, P.Y. Ayala, K. Morokuma, G.A. Voth, P. Salvador, J.J. Dannenberg, V.G. Zakrzewski, S. Dapprich, A.D. Daniels, M.C. Strain, O. Farkas, D.K. Malick, A.D. Rabuck, K. Raghavachari, J.B. Foresman, J.V. Ortiz, Q. Cui, A.G. Baboul, S. Clifford, J. Cioslowski, B.B. Stefanov, G. Liu, A. Liashenko, P. Piskorz, I. Komaromi, R.L. Martin, D.J. Fox, T. Keith, M.A. Al-Laham, C.Y. Peng, A. Nanayakkara, M. Challacombe, P.M.W. Gill, B. Johnson, W. Chen, M.W. Wong, C. Gonzalez, J.A. Pople, Gaussian 03, Revision E.01, Gaussian, Inc., Wallingford, CT, 2004.
[62] G. Karlström, R. Lindh, P.-Å. Malmqvist, B.O. Roos, U. Ryde, V. Veryazov, P.-O. Widmark, M. Cossi, B. Schimmelpfennig, P. Neogrady, L. Seijo, Comput. Mater. Sci. 28 (2003) 222.
[63] T.H. Dunning Jr., R.J. Harrison, J. Chem. Phys. 96 (1992) 6796.
[64] J.F. Stanton, R.J. Bartlett, J. Chem. Phys. 98 (1993) 7029.
[65] M.J. Frisch, G.W. Trucks, H.B. Schlegel, G.E. Scuseria, M.A. Robb, J.R. Cheeseman, G. Scalmani, V. Barone, B. Mennucci, G.A. Petersson, H. Nakatsuji, M. Caricato, X. Li, H.P. Hratchian, A.F. Izmaylov, J. Bloino, G. Zheng, J.L. Sonnenberg, M. Hada, M. Ehara, K. Toyota, R. Fukuda, J. Hasegawa, M. Ishida, T. Nakajima, Y. Honda, O. Kitao, H. Nakai, T. Vreven, J.A. Montgomery Jr., J.E. Peralta, F. Ogliaro, M. Bearpark, J. J. Heyd, E. Brothers, K.N. Kudin, V.N. Staroverov, R. Kobayashi, J. Normand, K. Raghavachari, A. Rendell, J.C. Burant, S.S. Iyengar, J. Tomasi, M. Cossi, N. Rega, J.M. Millam, M. Klene, J.E. Knox, J.B. Cross, V. Bakken, C. Adamo, J. Jaramillo, R. Gomperts, R.E. Stratmann, O. Yazyev, A.J. Austin, R. Cammi, C. Pomelli, J.W. Ochterski, R.L. Martin, K. Morokuma, V.G. Zakrzewski, G.A. Voth, P. Salvador, J.J. Dannenberg, S. Dapprich, A.D. Daniels, O. Farkas, J.B. Foresman, J.V. Ortiz, J. Cioslowski, D.J. Fox, Gaussian 09, Revision A.02, Gaussian, Inc., Wallingford, CT, 2009.
[66] S. Cradock, P.B. Liescheski, D.W.H. Rankin, H.E. Robertson, J. Am. Chem. Soc. 110 (1988) 2758.
[67] L. Fernholt, C. Rømming, Acta Chem. Scand. Ser. A 32 (1978) 271.
[68] M. Riese, J. Grotemeyer, Anal. Bioanal. Chem. 386 (2006) 59.
[69] R.C. Lord, A.L. Marston, F.A. Miller, Spectrochim. Acta 9 (1957) 113.
[70] M.P. Fülscher, K. Andersson, B.O. Roos, J. Phys. Chem. 96 (1992) 9204.
[71] W.J. Buma, M.C.J.M. Donckers, E.J.J. Groenen, J. Am. Chem. Soc. 114 (1992) 9544.
[72] R. Bauernschmitt, R. Ahlrichs, Chem. Phys. Lett. 256 (1996) 454.
[73] D.J. Tozer, R.D. Amos, N.C. Handy, B.O. Roos, L. Serrano-Andrés, Mol. Phys. 97 (1999) 859.
[74] R.L. Ellis, G. Kuehnlenz, H.H. Jaffé, Theor. Chim. Acta (Berl) 26 (1972) 131.
[75] D. Hegarty, M.A. Robb, Mol. Phys. 38 (1979) 1795.
[76] Z.-L. Cai, J.R. Reimers, J. Phys. Chem. A 109 (2005) 1576.
[77] H. Eyring, S.H. Lin, S.M. Lin, Basic Chemical Kinetics, Wiley, New York, 1980.